InAs/GaAs sharply-defined axial heterostructures in self–assisted nanowires

David Scarpellini,[†,‡] Claudio Somaschini,[†] Alexey Fedorov,[¶] Sergio Bietti,[†] Cesare Frigeri,[§] Vincenzo Grillo,[§,∥] Luca Esposito,[⊥] Marco Salvalaglio,[†] Anna Marzegalli,[†] Francesco Montalenti,[†] Emiliano Bonera,[†] Pier Gianni Medaglia,[‡] and Stefano Sanguinetti[*,†]

L–NESS and Dipartimento di Scienza dei Materiali, Universitá di degli Studi di Milano Bicocca, Milan, Italy, Dipartimento di Ingegneria Industriale, Universitá di Roma 'Tor Vergata', Rome, Italy, L–NESS and CNR-IFN, Como, Italy, Istituto CNR-IMEM, Parma, Italy, Centro CNR-S3-NANO, Modena, Italy, and L–NESS and Dipartimento di Fisica, Politecnico di Milano, Como, Italy

E-mail: stefano.sanguinetti@unimib.it

Abstract

We present the fabrication of axial InAs/GaAs nanowire heterostructures on silicon with atomically sharp interfaces by molecular beam epitaxy. Our method exploits the crystallization at low temperature, by As supply, of In droplets deposited on the top of GaAs NWs grown by the self-assisted (self-catalyzed) mode. Extensive characterization based on transmission

[*]To whom correspondence should be addressed
[†]L–NESS and Dipartimento di Scienza dei Materiali, Universitá di degli Studi di Milano Bicocca, Milan, Italy
[‡]Dipartimento di Ingegneria Industriale, Universitá di Roma 'Tor Vergata', Rome, Italy
[¶]L–NESS and CNR-IFN, Como, Italy
[§]Istituto CNR-IMEM, Parma, Italy
[∥]Centro CNR-S3-NANO, Modena, Italy
[⊥]L–NESS and Dipartimento di Fisica, Politecnico di Milano, Como, Italy

electron microscopy sets an upper limit for the InAs/GaAs interface thickness within few bi-layers ($\leq$ 1.5 nm). A detailed study of elastic/plastic strain relaxation at the interface is also presented, highlighting the role of nanowire lateral free surfaces.

Keywords

Semiconductor Nanowires, Self–Catalyzed Growth, InAs, GaAs, Heterostructure, Molecular Beam Epitaxy

Semiconductor nanowires (NWs) are considered one of the most promising technologies for the development of optoelectronic, nanoelectronic, and energy applications.[1–5] Thanks to the efficient strain relaxation at their free sidewalls,[6] NWs allow the integration of dissimilar semiconductors regardless of lattice mismatch, polar/nonpolar growth, and difference in thermal expansion coefficient. In this respect, III-V semiconductors represent a fundamental class of materials, owing to the wide variety of possible material combinations and their properties, such as direct band gaps and high carrier mobilities.

Recently, many examples of axial NW heterostructures have been realized by means of Au-seeded vapour-liquid-solid (VLS) growth.[7–10] Reports indicate that heterointerfaces with switch of the group III sublattice frequently show grading.[11–14] In particular, in the technologically relevant case of InAs/GaAs severe issues have been reported, such as dominant kinking and prevailing radial over the axial growth[13] or lateral shift of the Au catalyst droplet during the heterostructure formation.[15] While such issues have been solved recently in Au-seeded VLS in Metal Organic Vapour Phase Epitaxy (MOVPE),[16] atomically sharp interfaces have never been achieved so far in Molecular Beam Epitaxy (MBE), where an unintentional radial growth frequently dominates over axial growth.[17] Despite its success in fabricating sharp interfaces in III-V NWs, Au-seeded VLS leads to an unintentional incorporation of catalyst atoms during the growth with concentrations in the NW in the order of 10^{17} - 10^{18} cm^{-3}.[18] Such an incorporation of Au atoms is an important issue when producing high-quality NWs for advanced optoelectronic devices, as it may be detrimental to their performances.[19–21] Furthermore, the presence of Au particles in the system is not compatible with monolithic integration on silicon, because of both the high Si solubility in Au, leading to unwanted Si-doping of the NW, and the Au-enhanced wet-chemical etching of Si,[22] preventing post-growth treatment of the sample. All the listed problems are tackled by the development of self–catalyzed synthetic modes based on MBE, which do provide an alternative to the Au assisted growth of NWs.[23,24] However, in the self-assisted growth mode, the presence of a Ga droplet on top of the GaAs NWs strongly limits the compositional variation along the growth axis,[25] thus hindering the fabrication of axial heterostructures.

Here we introduce a technique which allows for the selective growth, on the NW tips, of III-V segments and thus the fabrication of axial InAs/GaAs NWs with atomically sharp interfaces in the self-assisted MBE mode. The lower GaAs segment was realized by the self–catalyzed method on Si (111) substrates[23,24] with a final step for the Ga droplet consumption and the creation of a flat top facet. The upper InAs section was created by temporally splitting the supply of In and As. First, In droplets were selectively deposited on top of the GaAs lower segment and solidified at low temperature. Then, As was supplied to convert solid In into InAs crystals. This last step of the procedure mimics the droplet epitaxy technique,[26] where a far from equilibrium growth mode is used to obtain nano-islands and quantum dots, even in lattice matched compound semiconductors.[27–32] By our method, we are able to avoid, by kinetically controlling the growth mode, the formation of an unintentional radial growth of InAs around GaAs and, thanks to the Ga droplet consumption, to switch between the two group-III sublattices within few bilayers, as confirmed by high resolution transmission electron microscopy (HRTEM), as well as by scanning transmission electron microscopy (STEM) with a high angle annular dark field (HAADF) detector. The presence of a sharp interface between GaAs and InAs, avoiding composition gradients, allowed the study of the strain relaxation process in the NW. We have observed that the strain present at the interface between the two materials is released both plastically, by the insertion of dislocations, and elastically, thanks to the NW free sidewalls. The interplay between the two mechanisms gives rise to a non–uniform distribution of misfit dislocations at the interface.

All the samples were grown in a MBE system on Si (111) wafers. Each substrate was cleaned in clean room environment by HF and piranha solution. After the subsequent formation of a silicon oxide layer by air exposure,[19] samples were degassed in the MBE chamber at 620 °C for 10 minutes to ensure a contamination-free surface. Our growth procedure to obtain atomically sharp InAs/GaAs interfaces can be summarized in four main steps (see Figure 1) :

a) GaAs NWs growth on Si (111) substrate using the self–catalyzed mode (Figure 1a);

b) Ga droplet consumption and formation of a flat top on the GaAs NWs (Figure 1b);

c) In deposition on the NW flat top in form of droplets (Figure 1c)

d) InAs segment formation at the top of the GaAs NW by arsenization of In (Figure 1d).

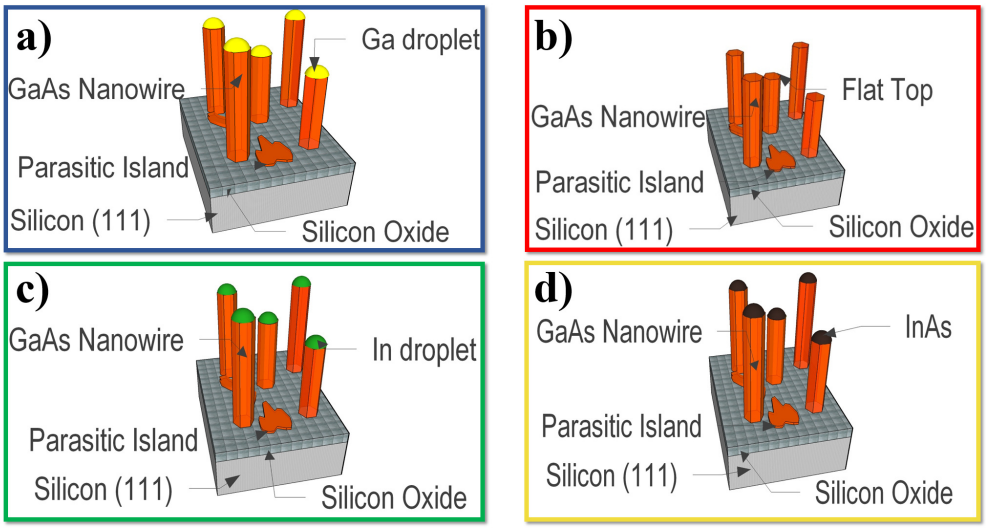

Figure 1: Process flow diagram of InAs/GaAs NWs grown on Silicon (111) substrate. (a) Growth of self-assisted GaAs NWs. (b) GaAs NWs with flat top facets achieved by consumption of Ga droplets. (c) In droplets deposited on top of the GaAs NWs. (d) InAs upper segment formation by arsenization of In.

The first step of the process was carried out at the substrate temperature of 580 °C, with a V/III ratio equal to 1. An As beam equivalent pressure (BEP) of 1.5×10^{-6} Torr was supplied to the substrate for 10 minutes and then, a Ga flux equivalent to 0.23 ML/s was provided to the substrate to initiate the NW nucleation. The growth was carried out for 40 minutes and led to the formation of the lower GaAs segment. After this step, we obtained the typical ensemble of GaAs NWs, with average diameter $D = 85 \pm 20$ nm, number density $\rho = (7 \pm 2) \times 10^8$ cm^{-2} and length around 2 μm. Figure 2a) shows the scanning electron microscope (SEM) image of a sample obtained stopping the growth at this stage. A Ga droplet is present at the top of each NW, as expected in the case of a self–catalyzed growth.[19,24,33]

The aim of the second step of our procedure is the formation of a flat top facet, by consuming the Ga droplet present on top of the GaAs NWs. For this purpose, the Ga shutter was closed, the As BEP set to 1×10^{-7} Torr and the substrate temperature reduced to 400 °C. The sample was

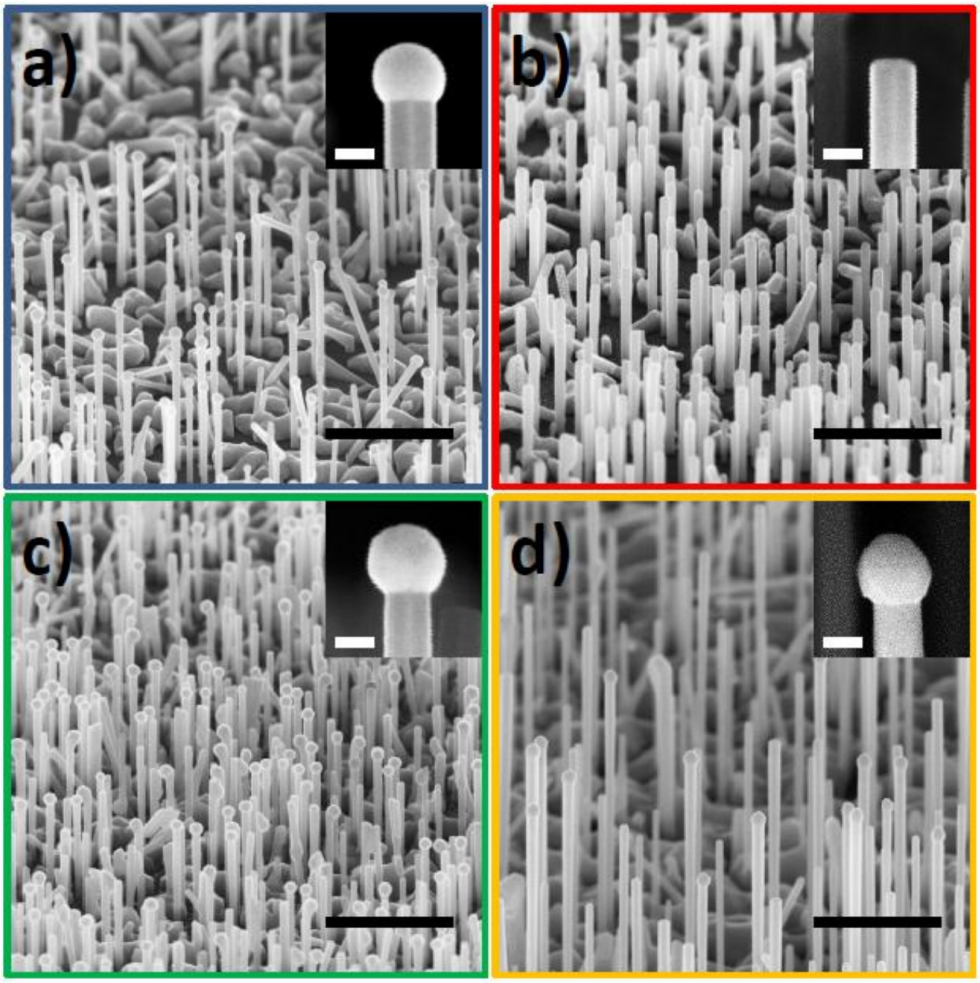

Figure 2: Low magnification SEM images obtained by tilting the holder at an angle of 30° and insets showing cross-section view along the top part of a single NW at high magnification . Scale bars are 2 μm and 100 nm, respectively. (a) GaAs NWs with Ga droplets clearly visible at their top. (b) GaAs NWs showing a flat top facet obtained by droplet consumption. (c) GaAs NWs with In droplets at their top. (d) InAs segment grown on top of the GaAs NWs.

kept under these conditions for one hour. This process allows a slow consumption of the droplet, promoting a layer-by-layer crystallization of GaAs, similarly to what is presented in Refs.[34,35] Figure 2b) shows the morphology of the NWs after the Ga droplet consumption, in a sample taken out from the growth chamber right after step 2. Interestingly, under these optimized conditions, there is not any noticeable change in the diameter of the NWs due to the consumption of the Ga, as observed in Refs.[34,36] The NWs exhibit a top facet parallel to the substrate, with a good surface flatness, as demonstrated by in–situ reflection high energy electron diffraction (RHEED) (see Supporting Information, S1).

In the third step of the growth process an In droplet was deposited on the top facet of the GaAs NW. Arsenic was depleted from the growth chamber down to a pressure below 10^{-9} Torr, maintaining the substrate temperature at 400°C. In order to be able to clearly image the In droplets by SEM, we deposited 100 MLs of In at a deposition rate of 0.05 ML/s and rapidly took the sample out from the MBE system. As shown in Figure 2c, In droplets were formed on top of the GaAs NWs. From the SEM image analysis, we estimated that around 30 % of the total amount of supplied In reached the top of the NWs. The remaining 70 % is likely to be captured by the parasitic growth, which is present on the substrate surface and provides additional nucleation centers for the In droplets. In addition to the sample prepared for clear SEM imaging (sample100), which is fabricated by supplying 100 MLs of In and is shown in Figure 2c, three additional samples with decreasing In coverage were realized for further characterization, namely 25 MLs (sample25), 12.5 MLs (sample12) and 6 MLs (sample6).

After In deposition, the substrate temperature was decreased to 100 °C. This caused the formation of a solid In crystal at the top of the NW. Then, an As BEP of 5×10^{-5} Torr was supplied for 5 minutes. Thereafter, under the same As pressure the substrate temperature was increased to 500 °C to ensure a good crystallinity of the InAs segment.[37,38] By this step (step four), InAs upper segments were realized on top of the GaAs NWs, therefore achieving the formation of axial InAs/GaAs NW heterostructure. The final morphology of sample100 is shown in Figure 2d) (the InAs segment morphology dependence on In coverage is reported in Supporting Information S2).

Such a low arsenization temperature (100 °C), similar to the value employed in the fabrication of InAs nano–islands on GaAs substrates by droplet epitaxy,[37] is dictated by the high diffusivity of In on GaAs around the In metallic droplet, thus hindering the realization of an axial heterostructure.[39] By reducing the substrate temperature, during As supply, below the In solidification temperature, we promoted a solid–solid transformation between In and InAs crystals, thus avoiding In diffusion from the In droplet to the NW side facets preventing NW radial growth mode.

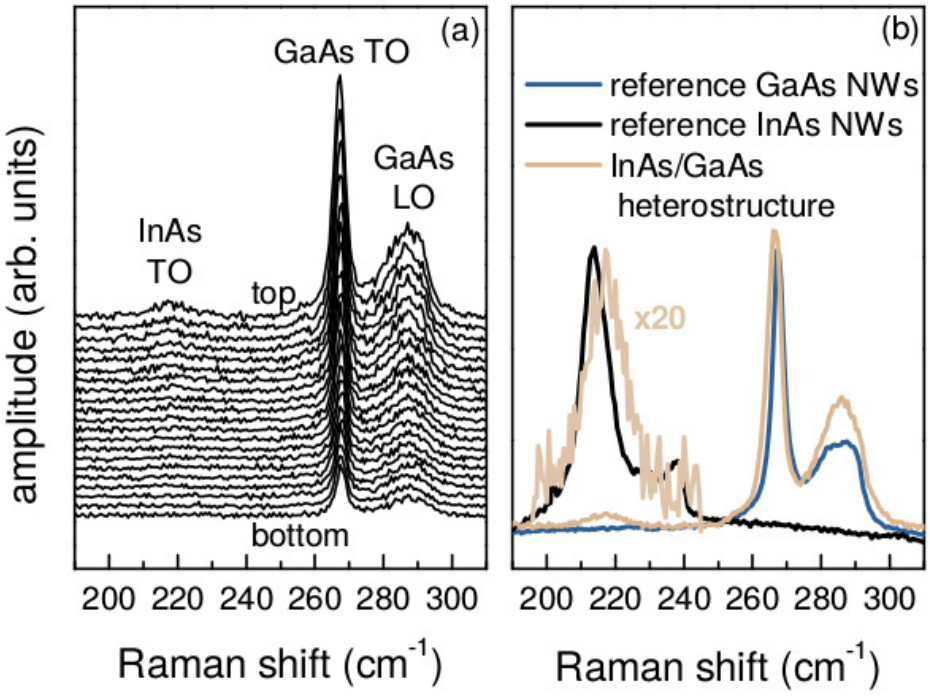

Figure 3: (a) InAs/GaAs Raman spectrum dependence on the position along the NW on sample25 after the arsenization process. (b) Comparison between the Raman spectra of InAs/GaAs NWs and of the reference pure GaAs NWs and pure InAs NWs.

To initially assess the local structural properties of the InAs/GaAs NW heterostructure, we performed measurements by Raman spectroscopy on sample25, after the arsenization procedure. The excitation wavelength was 532 nm (2.3 eV) and the excitation power was lowered until heating artifacts in the Raman spectra were not detectable (about 0.05 mW focussed by a 0.90 NA objective). The experiments were carried out by keeping the sample in cross section and measuring a small NW ensemble. By means of a micro-Raman setup, we scanned the wires from the bot-

tom (close to the substrate) to the top in steps of 0.1 μm, as shown in Figure 3a). The GaAs TO and LO bands are clearly observable in all the spectra at 267 and 287 cm^{-1} respectively.[40] Only when approaching the NW tip, a weak but detectable signal was observed at 217 cm^{-1},[41] which we attribute to the InAs segments, in agreement with our SEM analysis. Figure 3b) shows the superposition of the Raman spectrum from the InAs/GaAs NW heterostructures and the reference spectra of pure GaAs NWs and pure InAs NWs grown in the same system. The peaks related to GaAs and InAs are present only in sample25, containing the heterostructure and the coincidence between the InAs-related peak in sample25 and in the reference InAs NWs suggests the presence of relaxed InAs at the top of the NW. The InAs LO band was not detectable because of its low intensity.

To further investigate the microstructural properties of the axial InAs/GaAs NW heterostructures, TEM measurements were carried out on sample12 (obtained by supply of 12.5 MLs of In), using a Field Emission Gun (FEG) TEM/STEM JEOL 2200FS microscope working at 200 kV, operated in the conventional and HRTEM modes, as well as in the STEM mode with a HAADF detector with a camera length of 8 cm (collection angle of 75 mrad). The microscope has a point resolution of 0.19 and 0.136 nm in the TEM and STEM mode, respectively. STEM compositional maps of the NWs were obtained by X-ray Energy Dispersive Spectroscopy (X-EDS), from which elemental profiles were extracted. In the case of HAADF, the spot size was 0.2 nm, providing a very high spatial resolution. For the TEM analysis InAs/GaAs NWs were mechanically transferred on carbon-coated copper grids. In their lower segment, all analyzed NWs have $\langle 111 \rangle$ oriented zincblende (ZB) phase. The NWs are terminated by a segment of $\langle 0001 \rangle$ oriented GaAs wurzite (WZ) phase followed by a thin layer of $\langle 111 \rangle$ ZB GaAs, which is surmounted by the InAs crystal. The ZB and WZ parts are interfaced through a stripe of stacking faults and twins along the NW (not shown here). Polytypism in self-assisted GaAs NWs is a well-known phenomenon, already described in the literature.[42–44] In particular, the presence of segments of both polytypes at the top of the NW is usually observed when, as in our case, the Ga flux is switched off and the Ga droplet is consumed.[42,45] This behaviour has been attributed to the change in crystal nucleation

position which takes place during droplet consumption.[45] The upper InAs segment shows a slight predominance of ZB crystal structure, with a high number of stacking faults, as normally found out in MBE-grown InAs NWs.[46,47] The formation of InAs and the distribution of the group-III elements along the NW were investigated by high resolution STEM-HAADF , HRTEM and X-EDS. The resulting images are shown in Figure 4a) and 4b), whereas X-EDS is reported in the Supporting Information - S3. Examining figure 4a), we observed the presence of a stripe with higher brightness at the bottom of the InAs segment. Brighter areas in HAADF images can be related to the presence of strain centers, like misfit dislocations that are localised at the InAs/GaAs interface in our samples (see Figure 5), as they can increase the dechanneling.[48,49] However, according to the Z^n dependence of the HAADF contrast (Z atomic number, $1.7 < n < 2$), this effect can also be originated by an enrichment of In near the InAs/GaAs interface. In the following discussion, a detailed analysis of the interface morphology obtained by HRTEM will settle this doubt.

In Figure 4b) we show the HRTEM micrograph of the InAs/GaAs heterostructure, which confirms the high crystalline quality of the interface and the abrupt change in material composition, with interface sharpness at the atomic level, moving along the growth axis. The electron diffraction patterns from the upper InAs and lower GaAs segments, shown as insets, give a lattice spacing of d = 0.350 nm and d = 0.332 nm, respectively, for the arrowed spots corresponding closely to the $\langle 111 \rangle$ lattice spacings of pure InAs and pure GaAs. We do not observe the high local strain, related to the In-In bonds, 25% longer than the In-As bonds, which should be present in the case of an excess of In at the interface. Being the material switch between GaAs and InAs within few bilayers, we confirmed the success of our approach for the growth of axial InAs/GaAs NWs with sharp interfaces. Moreover, we should point out that in our experiments we did not observe any dependence of the morphology of the InAs/GaAs interface on the NW diameter ($D = 85 \pm 20$ nm), meaning that the obtained sharp interface is not related to the NW diameter, but rather relies on the crystallization at low temperature, by As supply, of solid In deposited at the top of the NW. This is in contrast with Au catalyzed NW growth,[16] where a dependence of the interface sharpness on the NW diameter is observed, because of the droplet reservoir effect.

Both Raman and TEM investigations point toward a complete relaxation of the strain in the InAs segment. Therefore, in agreement with theoretical calculations which predict plastic relaxation of strain for NW radii above around 20 nm,[6] a network of misfit dislocations is expected at the interface of the InAs/GaAs axial NW heterostructure. We investigated the presence of defects by studying the strain maps of the area near the heterointerface. HRTEM images were processed to determine spatial distribution and value of the strain by geometrical phase analysis (GPA),[50–52] using the STEM-CELL software package.[52] More details about the GPA method can be found in the Supporting Information (S4). Figure 5b) reports an image at high magnification of the strain map of the tip of the NW (shown in Figure 5a), evidencing different strain fields in InAs and GaAs. An ensemble of strain centers, due to misfit dislocations, is present and exactly located at the interface between GaAs and InAs. The correspondence between dislocation cores and the strain centers is demonstrated in Figure 5c) where the GPA strain map in the area of the strain center is overlapped to the corresponding HRTEM image before (left) and after (right) a Fourier filtering using the [11-1] Bragg vector. Clearly, an extra atomic plane is inserted at the strain center position perpendicularly to the interface plane, evidencing the edge geometry for the dislocations. The profile of the e_{xx} strain across the interface, obtained by integrating the strain values inside the black box area along the arrow in Figure 5b), is given in Figure 5d). The lattice parameter changes by 6.4 % when moving from GaAs (taken as reference) to InAs, which is consistent with the expected 7% lattice mismatch. The transition is not abrupt but occurs over a strained region about 2–3 nm wide in the NW axial direction. The dislocation network at the interface is then responsible for the strain relief in the InAs segment within a few nm from the interface. The presence of large strain gradients and misfit dislocations close ($\approx$ 2 nm) to the InAs/GaAs interface contributes to the formation of the brighter contrast we observed in HAADF at the bottom of the InAs segment, as mentioned earlier. The average lateral distance between dislocations is $\approx$ 5.2 nm. Interestingly, the strain map analysis revealed a radial dependence of the inter–dislocation distance (Figure 5e), which is increasing monotonically from the center to the sidewalls of the NW. Thanks to lateral relaxation, the same material can grow thicker on a given substrate as three dimensional island

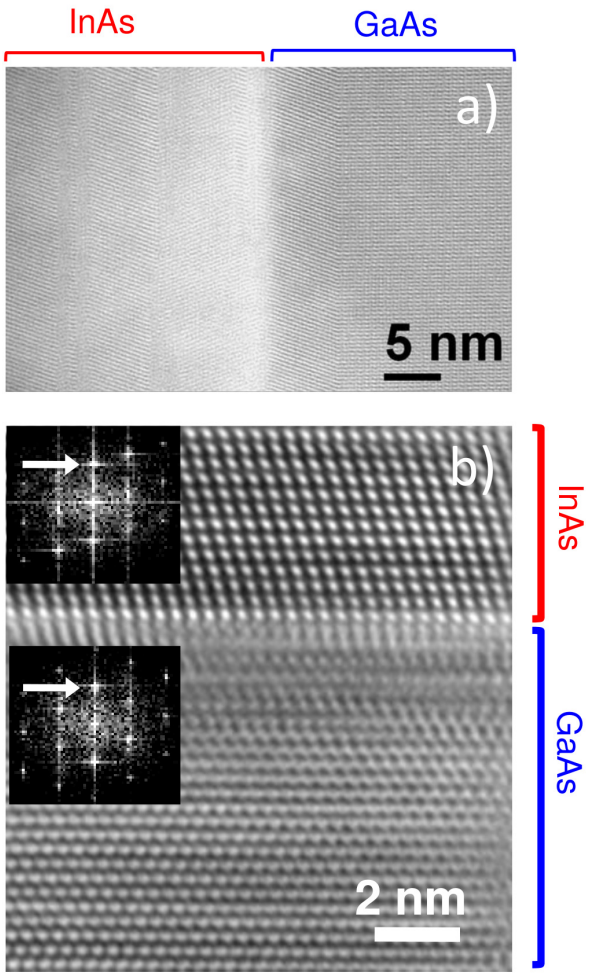

Figure 4: (a) High resolution STEM-HAADF image in the $\langle 110 \rangle$ zone axis of the InAs/GaAs NW tip, where InAs appears brighter and (b) HRTEM image in the $\langle 110 \rangle$ zone axis of the InAs/GaAs heterostructure, showing the atomically sharp interface. The electron diffractograms of InAs and ZB GaAs are shown as insets. In the insets the white arrowed $\langle 111 \rangle$ spot gives the corresponding lattice spacing of the two segments.

than as uniformly thick layer before the onset of plastic relaxation.[53] The critical thickness beyond which interfacial dislocations appear is therefore larger when strain relaxation is allowed through a free surface expansion.[54] For a misfitting layer at the top of a NW, lateral relaxation should be even more effective than for a three dimensional island, since it grows on a substrate which has the same finite diameter, thus being able to partially accommodate the lattice mismatch through deformation. As the position inside the NW moves from the NW center to the sidewall, a larger fraction of the strain should be relaxed elastically, through sidewall expansion, thus decreasing the amount of strain at the interface. In our case, the effect is sizeable, as the dislocation interdistance varies more than 30% while moving from the NW center to the periphery.

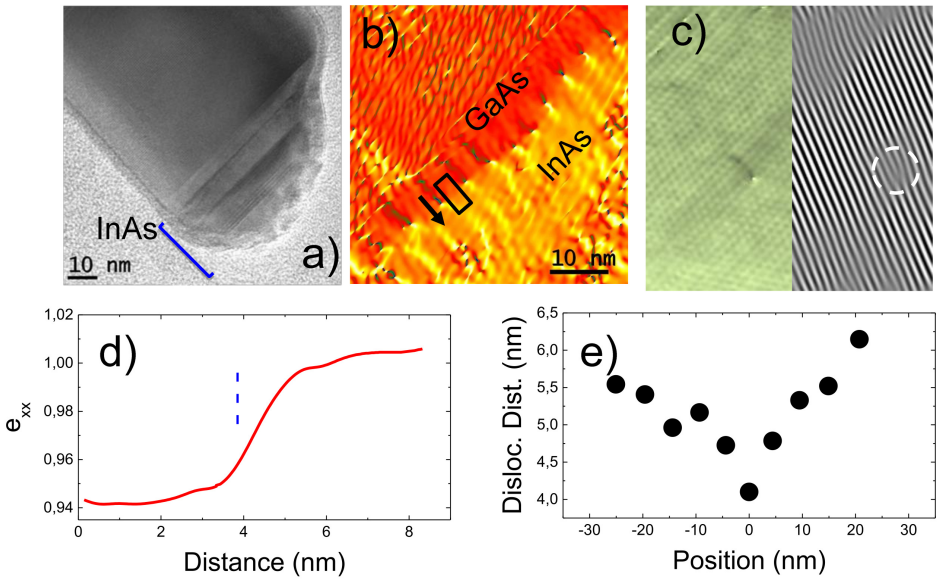

Figure 5: (a) TEM image of the tip of sample12. (b) Strain map of the InAs/GaAs interface at the tip of the NW (reported in (a)) at high magnification. (c) left: GPA strain map of a strain center overlapped to the corresponding HRTEM image. (c) right: HRTEM image after Fourier filtering displaying the extra half plane of the dislocation. (d) Strain profile, in the direction from GaAs to InAs, obtained by integrating the strain value within the black box in (b) along the direction indicated by the arrow between two dislocations. The vertical dashed blue line indicates the position of the interface. (e): Dependence of dislocation–dislocation distance on the position along the NW interface, measured from the NW center.

In order to better understand the coexistence of plastic and elastic relaxation in the NWs a theoretical analysis was carried out. The stress field in the coherent NW structure, shown in Figure 6a),

was calculated by numerically solving the elastic problem using finite element methods (FEM). The modulation induced by the free surfaces is evident. The upper InAs region is almost fully relaxed, while compressed and expanded stress-lobes are present around the interface. The effect of plastic relaxation was also investigated. To this end, a simplified procedure, analogous to the one presented in Ref.,[55,56] was exploited. While the coherent stress field was evaluated in 3D, the additional effect of plastic relaxation was computed in 2D, in a central slice of the heterostructure. Following the experimental evidence of Figure 5c, we considered dislocations of pure edge character. We should notice that their dislocation line in the actual system must be aligned along $< 112 >$ directions, as imposed by the $< 110 >\{111\}$ slip system and the $\{111\}$ interface orientation.[57] See Supporting Information S5 for more results and discussion.

In particular, we considered 11 dislocations placed at the InAs/GaAs interface, therefore mimicking the array revealed by HRTEM images (see Figures 5b and 5e). Exploiting a steepest-descent algorithm, we found their minimum-energy configuration by allowing moves along the horizontal direction. The resulting arrangement is shown in the color map of Figure 6b), while their spatial distribution is highlighted in Figure 6c). The latter qualitatively reproduces the experimental behavior, showing that the dislocation inter–distance is smaller in the InAs central region and larger at the edges. The model captures the behavior of the real system. This allows us to attribute the observed defect distribution to three driving forces: (i) mutual dislocation-dislocation interaction, (ii) effect of the free surfaces parallel to the dislocation lines, and (iii) interaction of the segments with the epitaxial elastic field. For a quantitative comparison, instead, a calculation including the description of the full 3D dislocation lines would be needed.

In conclusion, our growth method permits the realization by MBE of atomically sharp InAs/GaAs axial NW heterostructures on silicon. This result has been achieved by: i) self–catalyzed growth of GaAs NWs with a flat top, this property obtained by a dedicated Ga droplet consumption process; ii) selective deposition of InAs segments on the tips of the NW by a two step deposition process, where In nano–droplets are selectively formed on top of the GaAs NWs, solidified at low temperature and subsequently crystallized into InAs segments. This method, by kinetically limiting the

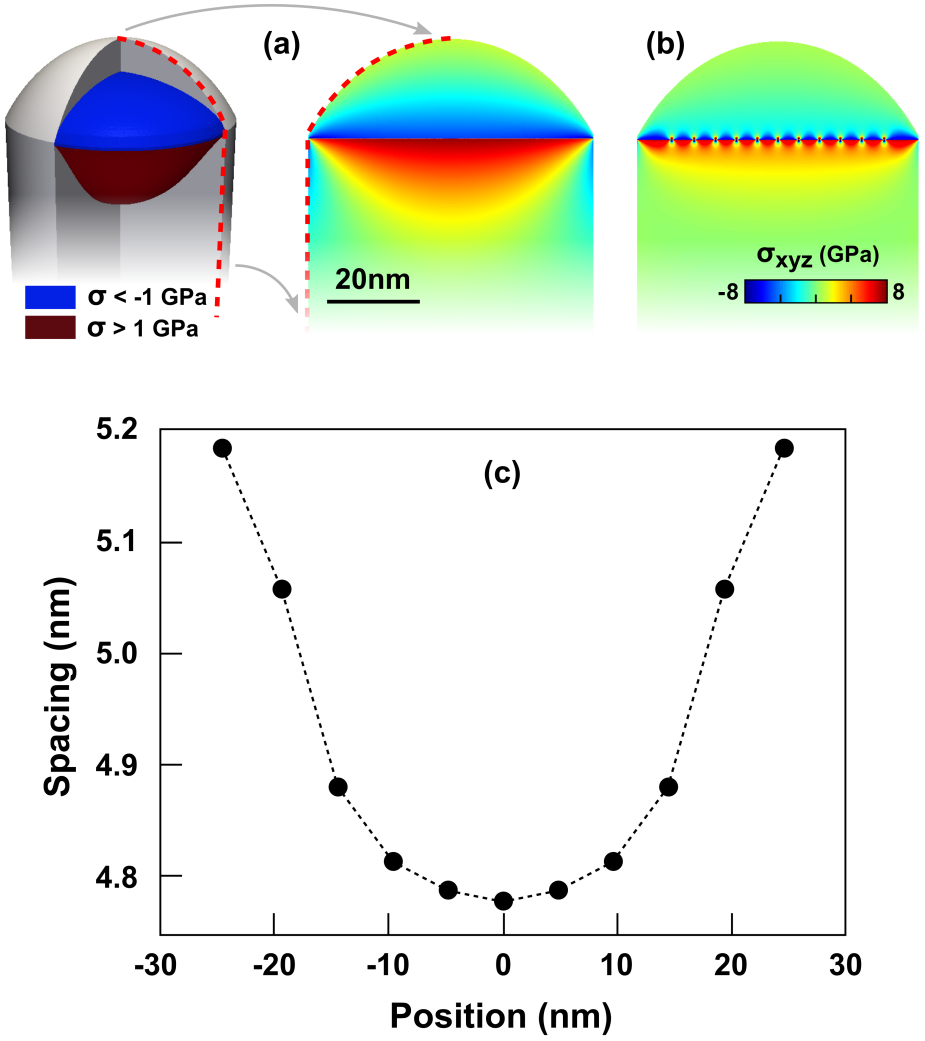

Figure 6: FEM calculation results for the relaxation in the InAs/GaAs heterostructure. The GaAs wire has been simulated cylindrical in shape with diameter equal to 65 nm, while the InAs dot above was built mimicking the shape experimentally observed (see Figure 5a). Panel (a): hydrostatic stress isosurfaces at 1GPa and -1 GPa in the three dimensional geometry (left) and hydrostatic stress color map in the central section (right). Panel (b): hydrostatic stress color map in the central section of a dislocated structure, for the minimum-energy configuration of 11 segments located at the interface (Burgers vector b=a/2(1-1 0) along (11-2)). Panel (c): spacing values between dislocation segments along the interface in the minimum-energy configuration

diffusion length of the In adatoms, avoids the formation of an unintentional radial growth of InAs. Extensive characterization by SEM, Raman spectroscopy and TEM confirmed the success of the method in terms of purely axial growth of InAs on GaAs and the atomically sharpness of the interface between the two materials. The thickness of our InAs/GaAs axial interface (i.e.< 1.5 nm) is comparable with the best report on the same NW heterostructure obtained using Au–assisted VLS NW growth, which shows In–Ga concentration gradients < 7 nm.[16] We obtained such a result in a fully catalyst-free growth mode, therefore eliminating the longstanding problem of Au incorporation into the wires. Hence, the proposed procedure first gives the possibility to produce high-quality wires for laser or transport devices,[18–21] whose performances are degraded by Au incorporation caused by Au-seeded VLS at high concentrations.[18] On the other hand the method can be extended to different III-V combinations, thus allowing the fabrication of stacks of multiple III-V axial heterostructures in the NW. For example, it could be possible to realize GaAs/InAs/GaAs NW double-heterostructures by positioning a Ga droplet, in the same way we performed with In, on the tip of the InAs/GaAs segment. Indeed, Priante et al.[35] have recently demonstrated that the presence of such a Ga droplet at the tip of the NW permits the resuming of the GaAs NW axial growth.

ASSOCIATED CONTENT

Supporting Information Available: Reflection high energy electron diffraction investigation of the Ga consumption step in GaAs self-assisted NWs, SEM investigation of the InAs segment morphology dependence on In coverage, X-EDS compositional information of InAs/GaAs MWs, Geometrical Phase Analysis details, FEM Strain Simulation details. This material is available free of charge via the Internet at http://pubs.acs.org.

Acknowledgement

We acknowledge partial financial support from Fondazione CARIPLO (Project EIDOS / 2011-0382)

References

(1) Huang, M. H.; Mao, S.; Feick, H.; Yan, H.; Wu, Y.; Kind, H.; Weber, E.; Russo, R.; Yang, P. *Science (80-.).* **2001**, *292*, 1897–9.

(2) Cui, Y.; Zhong, Z.; Wang, D.; Wang, W. U.; Lieber, C. M. *Nano Lett.* **2003**, *3*, 149–152.

(3) Gudiksen, M. S.; Lauhon, L. J.; Wang, J.; Smith, D. C.; Lieber, C. M. *Nature* **2002**, *415*, 617–20.

(4) Thelander, C.; Agarwal, P.; Brongersma, S.; Eymery, J.; Feiner, L.; Forchel, A.; Scheffler, M.; Riess, W.; Ohlsson, B.; Gösele, U.; Samuelson, L. *Mater. Today* **2006**, *9*, 28–35.

(5) Garnett, E.; Yang, P. *Nano Lett.* **2010**, *10*, 1082–7.

(6) Glas, F. *Phys. Rev. B* **2006**, *74*, 121302.

(7) Hyun, J. K.; Zhang, S.; Lauhon, L. J. *Annu. Rev. Mater. Res.* **2013**, *43*, 451–479.

(8) Minot, E.; Kelkensberg, F.; van Kouwen, M.; van Dam, J. A.; Kouwenhoven, L. P.; Zwiller, V.; Borgström, M. T.; Wunnicke, O.; Verheijen, M. A.; Bakkers, E. P. A. M. *Nano Lett.* **2007**, *7*, 367.

(9) Lim, S. K.; Crawford, S.; Haberfehlner, G.; Gradec, S. *Nano Lett.* **2013**, *13*, 331.

(10) Tchernycheva, M.; Cirlin, G. E.; Patriarche, G.; Travers, L.; Zwiller, V.; Perinetti, U.; Harmand, J.-C. *Nano Lett.* **2007**, *7*, 1500–4.

(11) Krogstrup, P.; Yamasaki, J.; Sø rensen, C. B.; Johnson, E.; Wagner, J. B.; Pennington, R.; Aagesen, M.; Tanaka, N.; Nygå rd, J. *Nano Lett.* **2009**, *9*, 3689–93.

(12) Paladugu, M.; Zou, J.; Guo, Y.-N.; Zhang, X.; Kim, Y.; Joyce, H. J.; Gao, Q.; Tan, H. H.; Jagadish, C. *Appl. Phys. Lett.* **2008**, *93*, 101911.

(13) Messing, M. E.; Wong-Leung, J.; Zanolli, Z.; Joyce, H. J.; Tan, H. H.; Gao, Q.; Wallenberg, L. R.; Johansson, J.; Jagadish, C. *Nano Lett.* **2011**, *11*, 3899–905.

(14) Venkatesan, S.; Madsen, M. H.; Schmid, H.; Krogstrup, P.; Johnson, E.; Scheu, C. *Appl. Phys. Lett.* **2013**, *103*, 063106.

(15) Paladugu, M.; Zou, J.; Guo, Y.-N.; Auchterlonie, G. J.; Joyce, H. J.; Gao, Q.; Hoe Tan, H.; Jagadish, C.; Kim, Y. *Small* **2007**, *3*, 1873–1877.

(16) Dick, K. A.; Bolinsson, J.; Borg, B. M.; Johansson, J. *Nano Lett.* **2012**, *12*, 3200.

(17) Heiss, M.; Ketterer, B.; Uccelli, E.; Morante, J. R.; Arbiol, J.; Fontcuberta i Morral, A. *Nanotechnology* **2011**, *22*, 195601.

(18) Bar-Sadan, M.; Barthel, J.; Shtrikman, H.; Houben, L. *Nano Lett.* **2012**, *12*, 2352–2356.

(19) Breuer, S.; Pfüller, C.; Flissikowski, T.; Brandt, O.; Grahn, H. T.; Geelhaar, L.; Riechert, H. *Nano Lett.* **2011**, *11*, 1276–9.

(20) Jiang, N.; Gao, Q.; Parkinson, P.; Wong-Leung, J.; Mokkapati, S.; Breuer, S.; Tan, H. H.; Zheng, C. L.; Etheridge, J.; Jagadish, C. *Nano Lett.* **2013**, *13*, 5135–5140.

(21) Gao, Q.; Saxena, D.; Wang, F.; Fu, L.; Mokkapati, S.; Guo, Y.; Li, L.; Wong-Leung, J.; Caroff, P.; Tan, H. H.; Jagadish, C. *Nano Lett.* **2014**,

(22) Lee, C.-L.; Tsujino, K.; Kanda, Y.; Ikeda, S.; Matsumura, M. *J. Mater. Chem.* **2008**, *18*, 1015.

(23) Fontcuberta i Morral, a.; Colombo, C.; Abstreiter, G.; Arbiol, J.; Morante, J. R. *Appl. Phys. Lett.* **2008**, *92*, 063112.

(24) Jabeen, F.; Grillo, V.; Rubini, S.; Martelli, F. *Nanotechnology* **2008**, *19*, 275711.

(25) Heiss, M.; Gustafsson, A.; Conesa-Boj, S.; Peiró, F.; Morante, J. R.; Abstreiter, G.; Arbiol, J.; Samuelson, L.; Fontcuberta i Morral, A. *Nanotechnology* **2009**, *20*, 075603.

(26) Koguchi, N.; Takahashi, S.; Chikyow, T. *J. Cryst. Growth* **1991**, *111*, 688–692.

(27) Watanabe, K.; Koguchi, N.; Gotoh, Y. *Jpn. J. Appl. Phys.* **2000**, *39*, L79.

(28) Kuroda, T.; Sanguinetti, S.; Gurioli, M.; Watanabe, K.; Minami, F.; Koguchi, N. *Phys. Rev. B* **2002**, *66*, 121302(R).

(29) Somaschini, C.; Bietti, S.; Koguchi, N.; Sanguinetti, S. *Nano Lett.* **2009**, *9*, 3419.

(30) Bietti, S.; Somaschini, C.; Koguchi, N.; Frigeri, C.; Sanguinetti, S. *J. Cryst. Growth* **2011**, *323*, 267.

(31) Somaschini, C.; Bietti, S.; Scaccabarozzi, A.; Grilli, E.; Sanguinetti, S. *Cryst. Growth Des.* **2012**, *12*, 1180–1184.

(32) Reyes, K.; Smereka, P.; Nothern, D.; Millunchick, J. M.; Bietti, S.; Somaschini, C.; Sanguinetti, S.; Frigeri, C. *Phys. Rev. B* **2013**, *87*, 165406.

(33) Fontcuberta i Morral, A.; Colombo, C.; Abstreiter, G.; Arbiol, J.; Morante, J. R. *Appl. Phys. Lett.* **2008**, *92*, 063112.

(34) Heon Kim, Y.; Woo Park, D.; Jun Lee, S. *Appl. Phys. Lett.* **2012**, *100*, 033117.

(35) Priante, G.; Ambrosini, S.; Dubrovskii, V. G.; Franciosi, A.; Rubini, S. *Cryst. Growth Des.* **2013**, *13*, 3976–3984.

(36) Dimakis, E.; Ramsteiner, M.; Tahraoui, A.; Riechert, H.; Geelhaar, L. *Nano Res.* **2012**, *5*, 796–804.

(37) Urbańczyk, A.; Hamhuis, G. J.; Nötzel, R. *Appl. Phys. Lett.* **2010**, *97*, 043105.

(38) Urbańczyk, A.; Keizer, J. G.; Koenraad, P. M.; Nötzel, R. *Appl. Phys. Lett.* **2013**, *102*, 073103.

(39) Noda, T.; Mano, T.; Sakaki, H. *Cryst. Growth Des.* **2011**, *11*, 726–728.

(40) Zardo, I.; Conesa-Boj, S.; Peiro, F.; Morante, J. R.; Arbiol, J.; Uccelli, E.; Abstreiter, G.; Fontcuberta i Morral, a. *Phys. Rev. B* **2009**, *80*, 245324.

(41) Begum, N.; Piccin, M.; Jabeen, F.; Bais, G.; Rubini, S.; Martelli, F.; Bhatti, A. S. *J. Appl. Phys.* **2008**, *104*, 104311.

(42) Yu, X.; Wang, H.; Lu, J.; Zhao, J.; Misuraca, J.; Xiong, P.; von Molnár, S. *Nano Lett.* **2012**, *12*, 5436.

(43) Rudolph, D.; Hertenberger, S.; Bolte, S.; Paosangthong, W.; Markus, D.; Bichler, M.; Finley, J. J.; Abstreiter, G.; Koblmüeller, G. *Nano Lett.* **2011**, *11*, 3848.

(44) Spirkoska, D. et al. *Phys. Rev. B* **2009**, *80*, 1–9.

(45) Krogstrup, P.; Curiotto, S.; Johnson, E.; Aagesen, M.; Nygå rd, J.; Chatain, D. *Phys. Rev. Lett.* **2011**, *106*, 1–4.

(46) Dimakis, E.; Jonas, L.; Jahn, U.; Hilse, M.; Geelhaar, L. *Cryst. Growth Des.* **2011**, *11*, 4001.

(47) Koblmüller, G.; Hertenberger, S.; Vizbaras, K.; Bichler, M.; Bao, F.; Zhang, J.-P.; Abstreiter, G. *Nanotechnology* **2010**, *21*, 365602.

(48) Phillips, P.; De Graef, M.; Kovarik, L.; Agrawal, A.; Windl, W.; Mills, M. *Ultramicroscopy* **2012**, *116*, 47–55.

(49) Grillo, V.; Rossi, F. *J. Cryst. Growth* **2011**, *318*, 1151–1156.

(50) Hÿtch, M. J.; Snoeck, E.; Kilaas, R. *Ultramicroscopy* **1998**, *74*, 131–146.

(51) Hÿtch, M. J.; Putaux, J. L.; Pennison, J. M. *Nature* **2003**, *423*, 270-273.

(52) Grillo, V.; Rossi, F. *Ultramicroscopy* **2013**, *125*, 112–29.

(53) Eaglesham, D.; Cerullo, M. *Phys. Rev. Lett.* **1990**, *64*, 1943.

(54) Mathews, J.; Blakeslee, A. *J. Cryst. Growth* **1974**, *27*, 118–125.

(55) Salvalaglio, M.; Montalenti, F. *J. Appl. Phys.* **2014**, *116*, 104306.

(56) Montalenti, F.; Salvalaglio, M.; Marzegalli, A.; Zaumseil, P.; Capellini, G.; Schülli, T. U.; Schubert, M. A.; Yamamoto, Y.; Tillack, B.; Schroeder, T. *Phys. Rev. B* **2014**, *89*, 014101.

(57) Zepeda-Ruiz, L. A.; Maroudas, D.; Weinberg, W. *Surf. Sci.* **1998**, *418*, L68–L72.

Graphical TOC Entry